ORIGINAL PAPER

A new Modified Heterocyclic-Magnetite Chitosan Nanocomposite for Efficient Alizarin Red Dye Removal: Adsorption Analysis and Antibacterial Activity

Asmaa Abuessawy[1,2] · Amr Fouda[3] · Adel A.-H. Abdel-Rahman[1] · Mohamed A. Hawata[1] · Nora A. Hamad[1]

Abstract
Alizarin Red (AR) is one of the most colored hazardous industrial dyes. For effective removal of AR, a new sorbent of modified heterocyclic-magnetite chitosan nanocomposite labeled as AOC@MC was synthesized and characterized by FTIR, TGA, XRD, BET, TEM,SAED pattern and SEM-EDX. Effect of contact time, pH, adsorbent dosage, initial Alizarine Red concentration and temperature was investigated. The maximum AR removal was 98.9% and attained at optimum conditions which were pH = 3.0, contact time = 50 min., and adsorbent dosage = 0.03 g/L. The findings revealed that at pH 3 and 30 °C, the maximum adsorption capacity was approximately 162 mg/g. Within 50 min, equilibrium adsorption was attained. A pseudo-second-order equation might be used to fit the kinetic data that was acquired at the optimal pH level of 3. Langmuir adsorption isotherms could accurately represent the adsorption process. The antimicrobial properties of the functionalized sorbent AOC@MC and its heterocyclic base AOC were characterized by determining the zone of inhibition (ZOI) against *Staphylococcus aureus* and *Klebsiella pneumonia* as a model for Gram-positive and Gram-negative bacteria respectively. AOC@MC exhibits promising activity with clear zones of 20.1 ± 0.2 and 17.6 ± 0.4 mm for *S. aureus* and *K. pneumonia* respectively. Overall, the modified sorbent AOC@MC was efficient on AR dye removal and antibacterial activity compared to the corresponding heterocyclic compound AOC.

Keywords Magnetite chitosan · functionalized nanocomposites · Alizarin red · Dye removal · Antibacterial activity

Introduction

Because of the rapid advanced progress in industry and technology our global environment is daily subjected to massive amounts of industrial effluents [1, 2]. Large quantities of hazardous are included in these effluents. Today, it is expected that 1.6 million tonnes of dyes are produced annually. These colored contaminants or dyes are widely employed across a variety of industries including textile, paper, plastics, marine, culinary, paints, and coatings [3–5]. Dyes effluents that resulted from most industrial sectors are usually drainage into wades, rivers, seas, and oceans. These non-biodegradable industrial effluents cause permanent contamination of the environment which in turn affects the typical ecological system badly by changing the color and odor of the natural water resources [6, 7]. Dyes are mostly carcinogens and cause many diseases such as skin irritation, dermatitis, mutations, allergies, and cancer in both animals and humans. The aqueous solutions which contains a significant amounts of unused dyes that have been released into

✉ Nora A. Hamad
    nhamad059@gmail.com

Asmaa Abuessawy
a.abuessawy@science.menofia.edu.eg

Amr Fouda
amr_fh83@azhar.edu.eg

Adel A.-H. Abdel-Rahman
adelnassar63@yahoo.com

Mohamed A. Hawata
drmohamedhawata@gmail.com

1   Chemistry Department, Faculty of Science, Menofia University, Shebin El-Kom 32511, Egypt

2   Basic Science Department, Higher Institute of Engineering and Technology, Menoufia, Egypt

3   Botany and Microbiology Department, Faculty of Science, Al-Azhar University, Nasr City 11884, Cairo, Egypt

water bodies by various industries pose a serious threat to the aquatic environment by consuming oxygen and increasing biochemical oxygen demand [8–10].

Dyes are can be divided into synthetic and natural dyes (from plants, animals, and minerals), but synthetic ones are the most widely used. Their structure includes auxochromes and chromophores and their molecular structure is aromatic due to hydrocarbon skeleton. The electron receivers that impart color are chromophores, while auxochromes are the electron donors which intensify colors onto the substrate [11, 12]. According to their particular charge dyes can also be classified into anionic, cationic, and non-ionic dyes. Based on their chemical structure dyes are divided into anthraquinone dyes, azo dyes, indigo dyes, nitrosated dyes, xanthene dyes, diphenylmethane and triphenylmethane dyes [13, 14].

Anthraquinone dyes such as alizarin red (AR) are considered as the most durable dyes which cannot be completely degraded by general chemical, physical, and biological processes [15]. Alizarin Red (1,2-dihydroxy-9,10-anthraquinonesulfonic acid) is an anionic dye known for its toxicity, and carcinogenic effects and it may also cause some other health problems such as dermatitis [16]. It is a water-soluble dye, that acts as a color indicator (with a pKa 4.6–6.5) so that is usually used in food, textile, and dye industries, and in turn, it is found mostly in their effluents [17]. Therefore, based on the mentioned considerations, it is necessary to remove it from the contaminated wastewater [18]. There have been many reported techniques for removing colored pollutants from aquatic environments, such as coagulation and flocculation, membrane filtration, electrochemical oxidation, ion exchange, advanced oxidation and adsorption [4, 19]. One of the most recent effective techniques for dye removal is adsorption due to its operational simplicity and low energy costs [20]. Recently, the research progress in the synthesis and modification of chitosan-based polymer nanocomposites has been widely developed because of their unique mechanical and physicochemical properties which strongly qualify them to undergo various environmental applications [21, 22]. For example, it was illustrated that functionalized modified chitosan nanocomposites can improve chemical stability, sorbents porosity, and adsorption capacity [23–27].

In this study we synthesized a new modified low-cost heterocyclic-chitosan nanocomposite. The modified sorbent AOC@MC was successfully applied to effectively remove Alizarin Red from aqueous solutions. For a better comparison of the experimental data, the initial pH effects, kinetics, equilibrium, desorption, and a reusability study was also investigated. The antibacterial effect of both organic base and polymeric nanocomposite was examined against pathogenic bacteria using the disk diffusion technique. *Staphylococcus aureus* and *Klebsiella pneumoniae* were used as a model for Gram-positive and Gram-negative bacteria

respectively. Further applications in the treatment of actual waste effluents will benefit from this understanding.

Materials and Methods

Materials

Chitosan (acetylation degree, DA: 25%), epichlorohydrin (EPI, 98%), (DMF; 99.8%), Ethanol (99%), Sodium chloride, Acetone, $FeCl_3.6H_2O$ and $FeCl_2.4H_2O$ were purchased from Damao Chemical Agent Company (Tianjin, China), Alizarin Red was Obtained from merk (Shanghai, China). Acetyl acetone, cyanoacetamide, ethyl chloro acetate were purchased from Sigma-Aldrich (S.D. Fine Chemicals Ltd., 98% min. assay). Thio hydrocarbazide was prepared at the laboratory by the reaction of Hydrazine hydrate (NH2–NH2) with Carbon disulfide(S=C=S) in ice bath. Thin-layer chromatography (TLC) was used to follow the completion of the reaction with benzene and methanol mixture as the mobile phase (8:2 volume ratios). All other reagents used in this study were analytical grade from Damao Chemical Agent Company (Tianjin, China) and distilled or double distilled water was used in the preparation of all solutions.

Methods

Preparation of 4, 6-di methyl-2-oxo-1,2-di Hydropyridine-3-carbonitrile (1)

Sodium metal (1.53 g, 10 mmol) was added in small pieces to 200 ml of ethyl alcohol in a round-bottomed flask with cooling in an ice bath. When all sodium was dissolved, the solution was brought to 25 °C to form sodium ethoxide then add a mixture of 6.9 ml, 69 mmol) acetyl acetone with (5.7 g, 67.8 mmol) of cyanoacetamide. The mixture was refluxed at 80 °C for 8 h, and a precipitate was formed after pouring onto crushed ice which was filtered off, washed with water, and dried well to give compound 1. (Scheme S1). The crude product was recrystallized from ethanol (final weight = 7 g in 70% yield).

Preparation of Ethyl 2-(3-cyano-4,6-dimethyl–2-oxopyridine-1(2 H)-yl)acetate (2)

Ethyl chloroacetate (1.65 g, 13.4 mmol) was added dropwise to a well-stirred solution of compound 1 (2 g, 13.5 mmol) in DMF (50 ml), potassium hydroxide (0.8 g, 14.2 mmol). The reaction mixture was stirred at 60–65 °C for 12 h, then cooled to room temperature and poured onto ice bath with stirring (removal of excess KOH) (Scheme S1). The precipitated compound (**2**) was filtered, washed with water, dried, and separated using column chromatography (methylene

chloride followed by methylene chloride, ethyl acetate mixture) the separated compounds obtained after vaporization of solvent were recrystallized from ethanol (final weight = 2.5 g with 80.6% yield).

Preparation of 1-((4-amino-5-thioxo-4,5-dihydro-1 H-1,2,4-triazole-3-yl)Methyl)-4,6-dimethyl-2-oxo-1,2-dihydropyridine-3-carbonitrile (3) OAC

A mixture of compound **2** (7 g, 30 mmol) and thiocarbazide (3.1 g, 29.2 mmol) in sodium methoxide (0.69 g, 4.5 mmol of sodium in 50 ml methanol) was refluxed at 70 °C for 17 h. A precipitate of compound 3 (**OAC**) was formed after pouring onto crushed ice then filtered off, washed with water, and dried well (Scheme S1). The crude product was recrystallized from ethanol (final weight = 8 g with 97.5% yield).

Preparation of Magnetite Nanoparticles (MC)

Magnetite nanoparticles were synthesized via the thermal co-precipitation reaction of ferrous sulphate ($FeSO_4.7H_2O$, 5.0 g) and hydrated ammonium ferric sulphate ($(NH_4)Fe(SO_4)_2.12H_2O$, 17.35 g) in water [28]. After vigorous stirring for 60 min at 40–50 °C, the pH was adjusted to 10–12 using 5 M NaOH solution keeping the mixture at 45 °C for 5 h. The magnetite nanoparticles were first separated magnetically, then washed in acetone and Milli-Q water, and then dried at 50 °C overnight. Chitosan powder (4 g) was soaked in acetic acid solution (150 mL, 20% w/w). To the chitosan solution, we added 1.5 g of magnetite nanoparticles. The mixture was kept at 45 °C, and the pH was reduced to 10 using a 5 M NaOH solution to precipitate magnetic chitosan microparticles (MC). The mixture was aged at 90 °C for 2 h. Crosslinking was used to increase the chemical stability of the composite. MC particles were crosslinked with epichlorohydrin (EPI) in an alkaline medium of 0.01 M (0.067 M NaOH solution; pH 10). The detailed procedure is shown in our previous research [29].
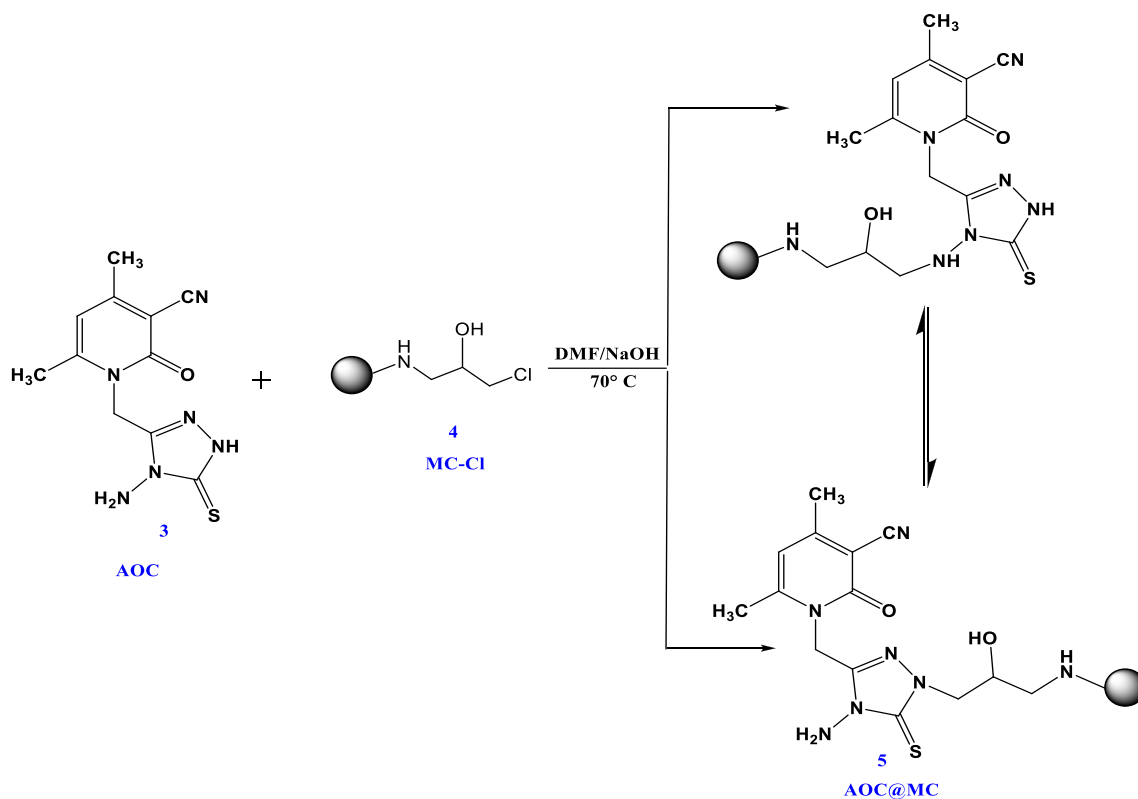
Preparation of MC-Cl (4) and AOC@MC

To a solution of MC 30 ml of epichlorohydrine in 200 ml of (ethanol/water) (1:1) was added. The mixture was stirred for 3 h at 70 °C. The precipitate of Mc-Cl was filtered, washed with ethanol, and dried at 50 °C to give MC-Cl (8.3 g). The synthesized heterocyclic compound 3 was added to 2.5 g of MC-Cl gram in 60 ml of DMF in a round-bottomed flask. The reaction mixture was refluxed for 9 h at 80 °C at pH 9.5 The AOC@MC precipitate was filtered, washed with water and ethanol, and dried at 50 °C (4.5 g) [30]. Scheme S2 and Scheme 1 summarize the different steps of the synthesis procedures.

Characterization of Materials

1 H-NMR (in DMSO-d5) and FTIR spectral analysis were used to confirm the structure of the synthesized heterocyclic compounds and polymeric sorbent. Using an alpha 100523 Jeol ECA 500 MHz NMR spectrometer,(Thermo Fischer Scientific, Inc., Waltham, MA, USA) 1 H-NMR analysis were operated .FTIR spectra were acquired using the so-called KBr disc method using an IRTracer-100 spectrophotometer (Shimadzu, Tokyo, Japan). Thermo gravimetric analysis (TGA) of was carried out in a nitrogen atmosphere using a Netzsch STA 449 F3 Jupiter thermogravimeter with a temperature ramp of 10 °C/min (under oxygen atmosphere) (NETZSCH-Ger¨ atebau GmbH, Selb, Germany).The morphology of AOC@MC before and after AR adsorption was investigated by Scanning Electron Microscope (SEM) using (SEM, Thermo Fisher Scientific, Netherlands) coupled with EDX facilities. The size and the morphological features were investigated adopting the high-resolution transmission electron microscope (HRTEM, JEOL-2100), The suspension of the material was sonicated for 20 min on an ultrasonicator (Crest Ultrasonics Corp., New Jersey, USA). Then few drops were loaded on carbon coated copper grid, left to dry, the grid loaded with the sample was examined by HR-TEM (JEOL, JEM-2100, Tokyo,Japan). The crystallinity of magnetite was characterized by X-ray diffraction patterns using an X-ray diffractometer X'Pert Pro (Philips, Eindhoven,Netherlands). The textural analysis of AOC@MC was carried out on a high-speed surface area analyzer (Nova-e Series, Model 25, Quantachrome, Kingsville, TX, USA). Brunauer − Emmett − Teller (BET) surface area analysis was carried out by using the nitrogen adsorption-desorption method (BELSORP MINI X, Microtrac BEL, Osaka, Japan).

Sorption Studies

A stock solution of Alizarin Red Dye (AR) (400 mg/L) was prepared. The additional solutions were made by diluting the stock solution with distilled water. Sorption measurements were performed at PH 1.0–7.0 and the pH using 0.1 M NaOH/HCl. 25 ml of each solution was combined with a weighted amount (30 mg) of the adsorbent, which was then agitated for 50 min at 250 rpm before being filtered. To determine the adsorption effectiveness of the prepared composite, the absorbance of AR solutions was measured using an evolution 300 ultraviolet-visible spectrophotometer at the wavelength of maximum adsorption (max= 423 nm). $q_e = (C_i - C_f)V/W_t$ Where W_t is the weight of the composite and V is the volume of AR in liters and W_t is the composite's weight in grams, q_e is its adsorption efficiency. The beginning and end AR concentrations are C_i and C_f, in milligrams per liter, respectively. The pHPZC values were determined by the pH-drift method [31].

Scheme 1 The preparation steps of AOC@MC

Evaluation of Antimicrobial Activity

The activity of synthesized compounds **OAC** and **AOC@MC** against pathogenic bacteria was investigated using the disk diffusion technique. *Staphylococcus aureus* ATCC 6538 and *Klebsiella pneumoniae* ATCC 700603 were used as a model for Gram-positive and Gram-negative bacteria respectively. In this method, the bacterial strain was subcultured in 100 mL of nutrient broth media (containing g L^{-1}: peptone, 5; beef extract, 3; and NaCl, 5, dH$_2$O, 1 L) and incubated for 24 h at 35 ± 2 °C. After that, 100 μL of bacterial culture (adjusted optical density at 1.0) was seeded into Muller-Hinton agar media (Oxiod, ready-prepared), shaking well, and poured into Petri dishes under aseptic conditions. After solidification, a paper disk (7 mm) was loaded with 100 μL of synthesized compounds (0.3 g/1ml DMSO) and lets it dry before being put on the surface of the seeded Muller-Hinton agar plate. Disks loaded with a solvent system (DMSO) were used as a negative control. The loaded plates were kept in the refrigerator for one hour to confirm complete diffusion before incubation at 35 ± 2 °C for 24 h. At the end of the incubation period, the results were recorded as a diameter of clear zone (mm) around each paper disk [32]. The experiment was achieved in triplicate. The clear zone was represented as a mean of three independent replicates $\pm$ standard deviation ($\pm$ SD).
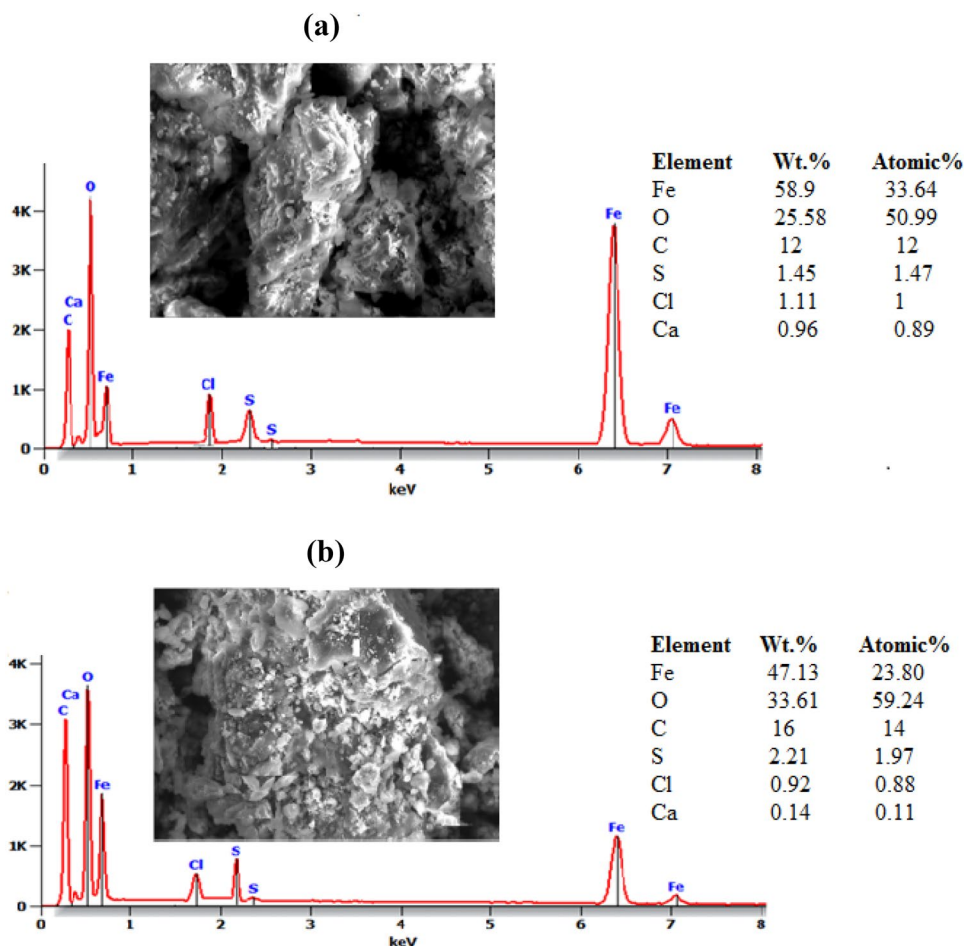
Results and Discussion

Characterization of Sorbents

Morphological Analysis SEM and TEM

The SEM picture of the AOC@MC (Fig. 1a) shows that the surface of nanoparticles is roughly shaped. The particles are also tightly packed together. According to its surface micrographs, the flake structure after adsorption may represent the AR coverage on AOC@MC MNPs (Fig. 1b). Typical EDX spectra along with elemental analysis results are displayed in (Fig. 1a, b). For the unused sample, EDX examination reveals the presence of various components including Fe (58.90%), O (25.58%), C (12%), S (1.45%), Cl (1.11%), and Ca (96%). The spectra show that Fe, O, and C are present, supporting the creation of magnetic chitosan particles. The fresh sample's Fe concentration was discovered to be 58.90% weight and 33.64% atomic. After removing the AR with AOC@MC, the Fe level dropped to 47.13% weight, and the increase in S (2.21% weight) confirmed that the AR dye had

(a)

Element	Wt.%	Atomic%
Fe	58.9	33.64
O	25.58	50.99
C	12	12
S	1.45	1.47
Cl	1.11	1
Ca	0.96	0.89

(b)

Element	Wt.%	Atomic%
Fe	47.13	23.80
O	33.61	59.24
C	16	14
S	2.21	1.97
Cl	0.92	0.88
Ca	0.14	0.11

been absorbed [33]. The TEM analysis and Selected Area Electron Diffraction (SAED) pattern are shown in (Fig. 2a–f) for AOC@MC and AOC respectively. (Fig. 2a, b) shows TEM for AOC@MC, the dark objects of magnetite nanoparticles (magnetite NPs,) is immobilized in the matrix of functionalized biopolymer (light-colored) can be observed with sizes ranging between (~ 4 and ~ 20 nm). The magnetite NPs are mostly distributed homogeneously showing irregular morphology and some are clustered in the form of agglomerates. (Fig. 2d, e) shows TEM for AOC, the particles size ranges between (~ 16 nm and ~ 54 nm). From the observed particles size of both AOC@MC and AOC the values indicates their formation as nanparticles which in turn illustrates the synthesis of AOC@MC nanocomposite. SAED pattern is a technique used alongside S/TEM to evaluate the sample's crystallinity, lattice parameters, and crystal structure and orientation by evaluating the electron diffraction pattern created by the electron beams interaction with the sample atoms. Depending on the type of sample, the SAED pattern can contain sharp spots from single crystal, ring patterns from nanocrystalline powders, or diffused ring patterns from amorphous samples [34]. Figure 2c shows SAED pattern of AOC@MC which exhibits ring patterns

that illustrated the formation of nanocrystalline magnetite NPs polymer composite while the pattern showed in Fig. 2f exhibits sharp spots indicating the single crystal morphology of AOC.

Textural Analysis-BET

The specific surface area ($a_{s,BET}$, m^2 g^{-1}), pore volume (V_p, cm^3 g^{-1}) and median pore diameter (nm) for AOC@MC were measured and were found to be 13.904 m2 g^{-1}, 0.086 cm^3 g^{-1} and 3.0648 nm respectively. The given values show that the textural properties of the sorbent were improved by the incorporation of magnetite NPs. (Fig. 3a, b) shows the BET plot and nitrogen adsorption−desorption isotherms at a temperature of 77 K. The hysteresis loop obtained from the graph suggests the type IV isotherm according to IUPAC classification, and the adsorbent is mesoporous.

Structural Analysis-XRD

By utilizing X-ray diffraction analysis (XRD) with Cu Kα radiation (λ = 0.1541 nm) at a rating of 40 KV, 40 mA, and 2θ ranging from 0 to 70° step duration 0.7 (s), the

Fig. 2 **a**, **b** TEM imagesof AOC@MC, **d**, **e** TEM imagesof OAC. SAED pattern, **c** SAED pattern of AOC@MC and **f** SAED pattern of AOC
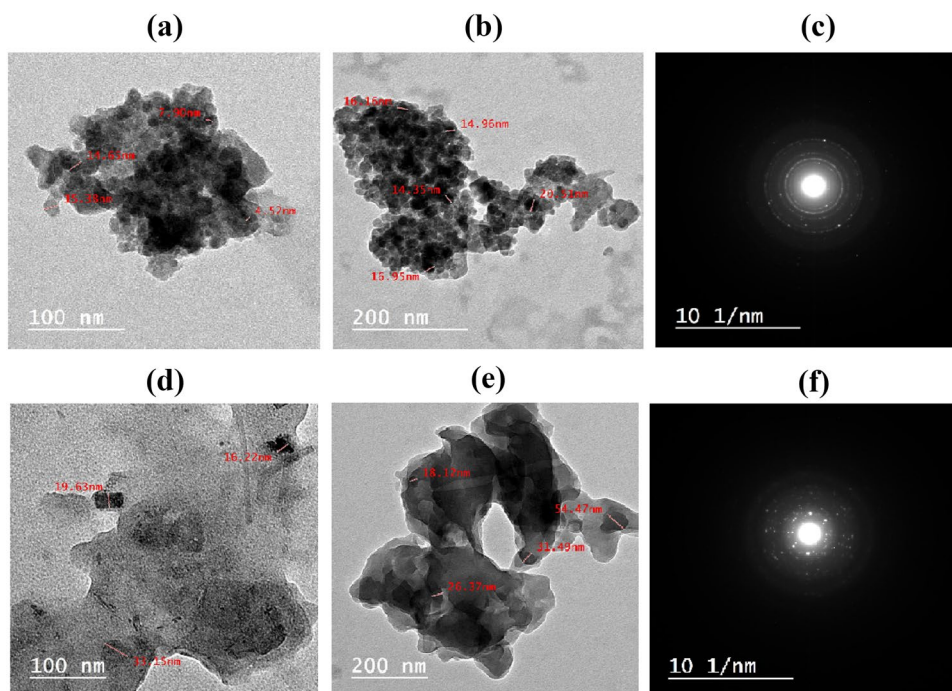
distribution of montmorillonite platelet in the chitosan matrix was investigated. The XRD diffraction pattern of AOC@MC is shown in Fig. 4 confirms the presence of magnetite NPs. with magnetic characteristics which may point to magnetic separation and confirming the intercalation of polymer composite. The characteristic peaks of Fe_3O_4 are ($2\theta = 30.11$, 35.5, 43.31and 53.42). Using the Pan Analytical X'pert PRO database from the International Centre for Diffraction Data, the produced crystalline phases were which is consistent with the order of magnitude of the NPs determined by TEM (Fig. 2).

Thermogravemtric Analysis

Chitosan was subjected to a thermogravimetric examination to confirm the existence of magnetic Fe_3O_4 (Fig. 5). At temperatures between 50 and 550 °C, weight loss occurs in two stages. At temperatures between 50 and 100 °C, the first stage entails desorption of water molecules that have been surface-adsorbed. Due to the dissolution of the polymer matrix, a nonlinear continuous decreasing weight was found at a higher temperature of 230 °C and persisted up to 520 °C.

FTIR Spectroscopy

FTIR was used to characterize the manufactured materials, with a scanning range of 4000 and 400 cm^{-1}. The characteristic peaks of chitosan can be seen in the infrared spectra of magnetic chitosan, including the adsorption band at 3414 cm^{-1} that reveals the stretching vibration of N–H

groups bonded with O–H groups in chitosan, the C–H bond at 2918 cm^{-1}, and the N–H scissoring from the primary amine in crosslinked chitosan at 1594 cm^{-1}. The effects of C–N stretching for primary amines and C–O stretching for the primary alcohol of chitosan are visible in bands between 1451 and 1383 cm^{-1}, respectively. At 577 cm^{-1}, the new magnetic chitosan peak is visible. It proves that magnetic particle surfaces developed a layer of chitosan. Fe_3O_4 nanoparticles in the magnetic chitosan are responsible for the Fe–O transverse vibrations at 577, 630, 797, and 895 cm^{-1} in the FTIR spectra (Fig. 6) and (Table 1). Both IR and H-NMR spectra of the prepared heterocyclic compounds **1, 2**, and **3 (AOC)** with their readings are shown (Fig. S5, S6). (See Supplementary Information).

Adsorption Experiments

Effect of pH

The pH of the aqueous solution is the most crucial factor in adsorption tests; it has a significant impact on the ability of beads to bind AR. The influence of pH on the sorption of AR on the produced absorbents is depicted in Fig. 7a. When pH decreased, the dye uptake is increased. In this study by adding 0.03 g of dry composite AOC@MC was to a series of flasks containing 25 ml of AR (200 mg/L) with different pH values (starting from 3 to 7), shaking at 250 rpm and 30 °C for 50 min, and filtering out, it was seen the maximum AR adsorption values, which were 162 mg/g.
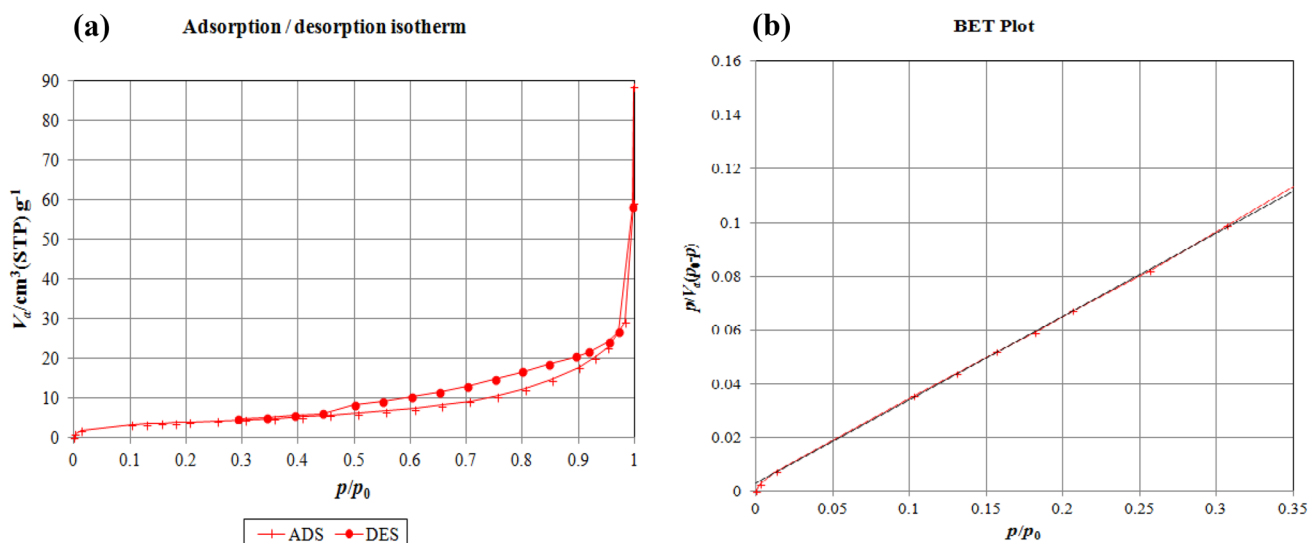
(a)

(b)

Fig. 3 BET surface area analysis of AOC@MC; **a** BET plot of the N 2 adsorption−desorption isotherm. **b** BET plot of N2 adsorption

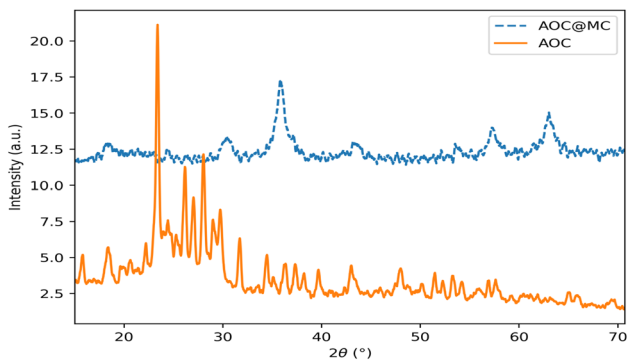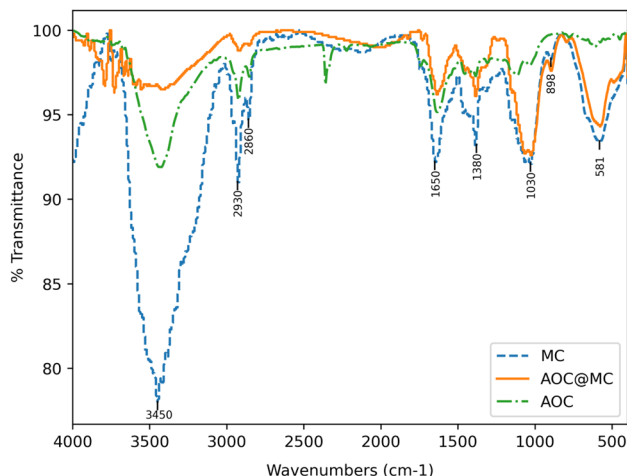Fig. 4 The XRD diffraction pattern of AOC@MC
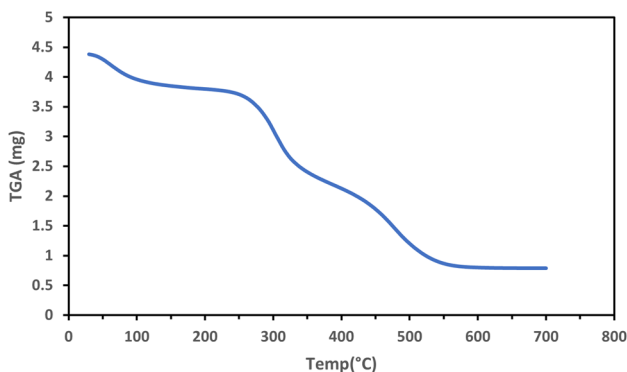

Fig. 6 IR of AOC and finial grafted sorbent AOC@MC

of AOC@MC composite were enclosed in a series of flasks each of which contained 25 mL of AR dye (200 mg/L), pH 3, then stirred at 250 rpm and 30 °C for 50 min and filtered off. Figure 7b illustrates the effect of AOC@MC dose on AR dye adsorption. The sorption capacity of AOC@MC was found to be reduced from 162 to 157.2 mg/g. The concentration difference between the sorbent and AR dye rises when the dosage is raised, resulting in aggregation and reduced dye transfer per unit mass onto the sorbent. Another factor contributing to the decreasing trend is the saturation of the adsorbent active pore site which reduced the dye molecule sorption. Therefore, we found that a dosage of 0.03 g/ 25 mL was the most effective for dye absorption.

Fig. 5 TGA analysis of AOC@MC

Effect of Sorbent Dose

Five different weights (0.03, 0.05, 0.07, 0.10 and 0.15) gm.

Table 1 FTIR assignment and wavelength (cm^{-1}) of MC, AOC and the finial grafted sorbent AOC@MC

Vibration	References	MC	AOC	AOC@MC
OH and NH$_2$ str. Overlapping	[35, 36]	3419	3425	3414
C–H aliphatic str. (Asymm. CH$_2$)	[37]	2925	2924	2918
C–H aliphatic str. (Symm. CH$_2$)		2856	2854	2856
C=O amide str. and (1°/2°)				
Amine bend. overlapping water molecules,	[38]	1646	1634	1636
C=C str.	[28, 39]			
Primary/Secondary amine bend.	[28, 39]		1592	1594
C–N, C–H and N–H str.		1462	1457	1451
C–H and (1°/2°) and OH bend., abd COO^- salt	[40, 41]	1384		1383
C–H bend., asymm. C–O–C str.	[37]	1317	1326	1325
Epoxy ring str.	[28]	1235		
C–O–C asymm. Str., C–C, C–O(CHOH) and C–N str.	[37]	1064, 1027		1064, 1025
β-D-glucose unit, CH$_2$ rock.	[42]	898		898
Fe$_{tetra}$ –O str	[37, 39]	581		577
Fe$_{octa}$ –O str	[40]	445		488

Effect of Temperature on the Extent of Adsorption

Four flasks containing 0.03 g of AOC@MC composite were filled with a total of 25 mL (200 mg/L and pH 3), and they were shaken for 50 min at various temperatures (20, 25, 30, and 40 °C). As indicated in Fig. 7c, the adsorption capacity increased from 159.7 to 162 mg/g as the temperature was raised. But at 40 °C, there was a decrease in the adsorption efficiency. This illustrates that lower temperature enhances adsorption while higher temperature enhances desorption.

Effect of Contact Time

By adding 0.03 g of dry composite to a series of flasks, the influence of time on the adsorption process was studied. Each flask contains 25 ml of 200 mg/L AR solution, is heated to 25 °C, has a pH of 3, and is swirled at various intervals. It was found that the maximum adsorption capacity occurs within 30 min, indicating rapid adsorption at the beginning of the reaction and its fast kinetics (Fig. 7d). During the first 30 min of the process, the adsorption capacity reached 94.4 mg/g. It was then increased to 96.7 mg/g by increasing the processing time to 50 min. After this step, the increase in contact time showed slight changes in adsorption capacity. Rapid adsorption at the beginning of the contact time is due to the large surface area available for dye adsorption. At this stage, adsorption will be essentially at the adsorbent surface. The adsorption process moves from the adsorbent particles' outer locations to the internal sites and slows down the process. According to the results, the equilibrium time for the AR removal was 50 min [43].

Effect of Adsorption Kinetics Studies

Figure 7d shows how the contact time affects the capacity of AR adsorption. Evidently, the adsorbent performed well within the first 60 min of adsorption. Only 50 min were needed to reach the adsorption equilibrium. After one hour, there was no discernible change. With the help of two kinetic models, the Lagergren pseudo-first-order and pseudo-second-order models, the adsorption kinetics of AR onto the modified sorbent AOC@MC are examined. One of the most used adsorption rate equations for solute adsorption from a liquid solution is the Lagergren rate equation.

Pseudo-First-Order Model The linear form is expressed as Eq. (1) [44]:

$$\log \left(q_e - q_t \right) = \log q_e - \frac{K_1}{2.303}t \tag{1}$$

Here, K_1 is the rate constant (1/min), t is the time of contact, and q_t and q_e are the adsorption capacities of the adsorbent during time t and at the equilibrium condition, respectively (min). Finding the values of K_1 and q_e is aided by the plot $\log\left(q_e - q_t\right)$ and t as shown in Fig. 8a.

Pseudo-Second-Order Model The adsorption kinetic model can be expressed in differential Eq. (2) [44]:

$$\frac{dq_t}{d_t} = K_2\left(q_e - q_t\right)^2 \tag{2}$$

where K_2 (g mg^{-1} min^{-1}) is the second-order rate constant, and the equation is simplified and can be re-written in a linear Eq. (3)
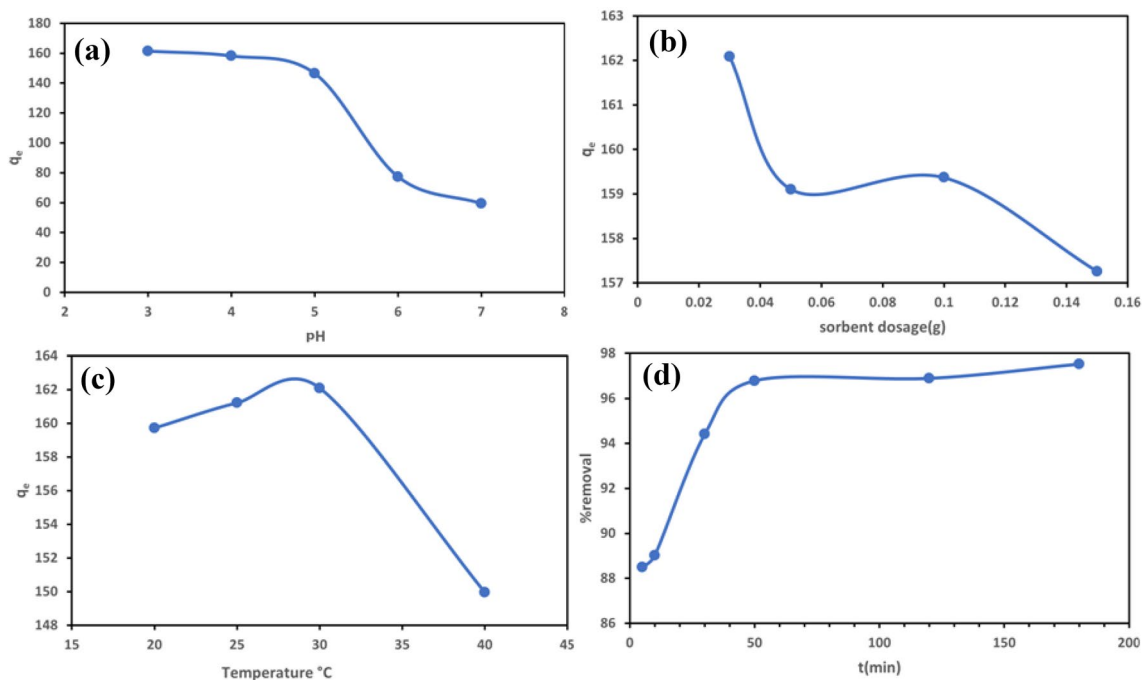
Fig. 7 Adsorption experiments **a** effect of pH on alizarin red adsorption, **b** effect of adsorbent dose on AR adsorption, **c** effect of Temperature on AR adsorption and **d** effect of time on Alizarin red adsorption

Table 2 Kinetic models for AR adsorption by AOC@MC

Kinetic model	Parameter	Definition	Value
Experimental	$q_{e,exp}(mg/g)$	Adsorp. cap. at t time	161.3
Pseudo-first-order	$q_{e,calc}(mg/g)$	Adsorp. cap. at equilibrium time	19.6
	$K_1(1/min)$	Rate const. for kinetic model	0.0525
	R^2		0.9796
Pseudo-second-order	$q_{e,calc}(mg/g)$	Adsorp. cap. at equilibrium time	163.9
	$K_2(1/min)$	Rate const. for kinetic model	0.007
	R^2		1
Intra-Particle diffusion	$K_i(mg/gmin^{-0.5})$	Rate const. of intra-particle diffusion	1.362
	I (mg/g)	Boundary layer thickness	146.8
	R^2		0.7727

$$\frac{t}{q_t} = \frac{1}{K_2 q_e^2} + \frac{1}{q_e}t \tag{3}$$

As indicated in Fig. 8b from the plot between $\frac{t}{q_t}$ and t, the values for K_2 and q_e are determined using the intercept and slope. The corresponding kinetic parameters from both models are listed in Table 2. The correlation coefficient (R_2) for the pseudo-second-order adsorption model has a high value (> 99%) for the adsorbent. The calculated equilibrium adsorption capacity of AOC@MC is 163.9 mg/g, which is consistent with the experimental data (162 mg/g) [45]. These facts suggested that the pseudo-second-order adsorption mechanism was predominant and that the overall rate of the

AR adsorption process appeared to be controlled by the chemisorptions process [46]. In addition, the optimum contact time for the adsorption of AR appeared to be 50 min. This could be attributed to the large surface area, the sufficient exposure of active sites, and the high surface reactivity of AOC@MC. The sorption of AR was rapid during the initial stages of the sorption process, followed by a gradual process. In the latter stages, however, the rate of AR adsorption became slower. The AR had to first encounter the boundary layer effect and then adsorb on the surface, and finally, they had to diffuse into the porous structure of the adsorbent which took a longer time.
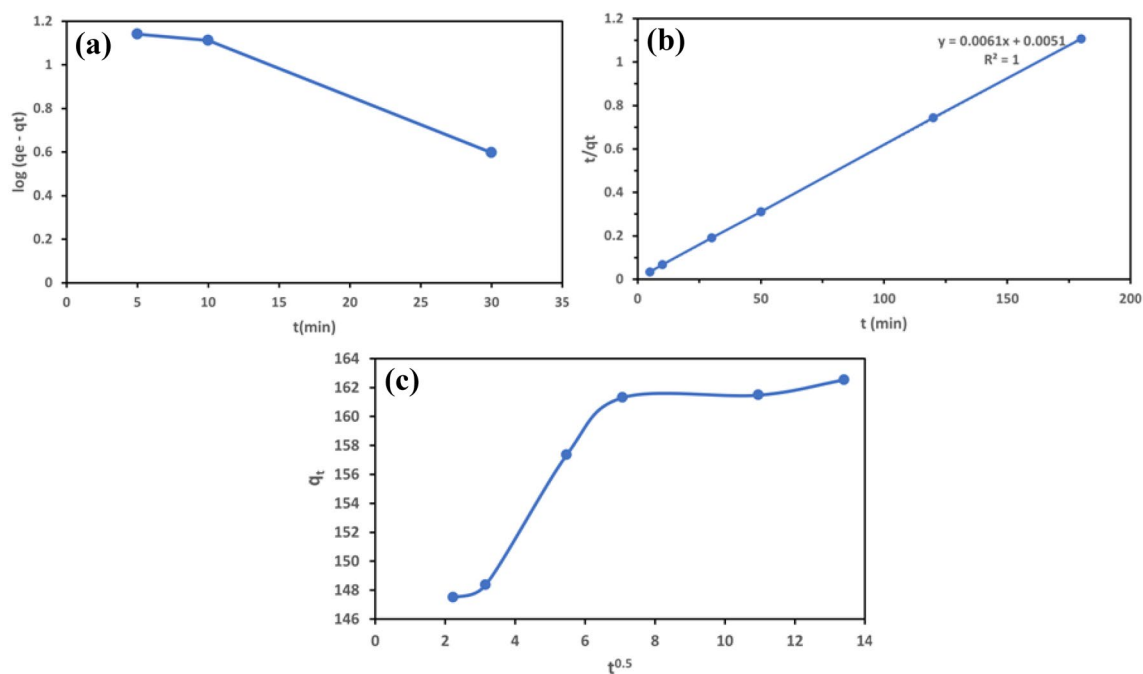
Fig. 8 Adsorption kinetic studies **a** Pseudo-first order kientic model, **b** Pseudo-second order kientic model and **c** Intra particle diffusion kinetic model

Intra-particle Diffusion The intra-particle diffusion model examined the kinetic results to clarify the diffusion mechanism. The three steps of (a) film or surface diffusion, in which the sorbate is transported from the bulk solution to the external surface of the sorbent, (b) intra-particle or pore diffusion, in which the sorbate molecules move into the interior of sorbent particles, and (c) adsorption on the interior sites of the sorbent, can be used to describe the overall rate of adsorption. It expresses the intraparticle diffusion model as follows Eq. (4)

$$q_t = K_i t^{0.5} + I \qquad (4)$$

where I is the intercept, K_i is the intra-particle diffusion rate constant in mg/(g min$^{1/2}$), and q_t is the amount of alizarin red adsorbed at equilibrium (mg/g) at time t. The slope and intercept of the plot of q_t vs. $t^{1/2}$ were used to compute the values of K_i and I for the intra-particle diffusion. If the linear plot passes through the origin, it shows that the intra-particle diffusion is the single factor limiting the rate of reaction. On the other hand, the surface sorption contributes more to the rate-limiting step; the larger the intercept is attained. Figure 8c depicts the intra-particle diffusion for AR adsorption by AOC@MC. The adsorption process's trend is identified throughout the adsorption process as three steps. The first step is the diffusion of the dye molecules via the boundary layer from the bulk solution to the modified chitosan composite's exterior surface. The second occurs when dye

molecules diffuse from the modified chitosan composite adsorbent's exterior surface into its pores. The ultimate equilibrium stage is when the dye molecules have been adsorbed on the active sites on the interior surface of the pore, and the intra-particle diffusion plot starts to slow down as the solute concentration in the solution decreases [47]. The surface adsorption mechanism predominately took place during the first 50 min of contact. The diffusion pathway thus became the rate-limiting stage. It was determined that the intra-particle diffusion rate constant kp (mg/g min$^{1/2}$). The intraparticle diffusion was not the only step that was rate-limited because the plot did not pass through the origin. As a result, only one process was rate limiting over a given time out of the three that affected the adsorption rate. The boundary layer effect is also shown by the plot's intercept. For the modified chitosan composite, we had a high value, which led to greater dye surface adsorption. As a result, the adsorption behaviors utilizing this adsorbent simultaneously combined surface adsorption and intra-particle diffusion mechanisms.

Evaluation of Adsorption Isotherm Models

Adsorption is a process in which adsorbate (dyes) is attached to the surface of the adsorbent as a result of various interactions between the adsorbent and adsorbate. Isotherm models are used in this case to identify how much adsorbate is present on the adsorbent's surface (or in the solid phase) and how much is left in the water sample (or in the liquid

Table 3 Langmuir, Freundlich, Temkin and D-R isotherm parameters for AR dye removal

Isotherm model	Parameter	Value	Definition
Langmuir	$q_m\left(\frac{mg}{g}\right)$	169.4	Maximum adsorption capacity
	$K_L\left(\frac{L}{mg}\right)$	2.68	The energy of adsorption
	R^2	0.9997	
Freundlich	$K_F\left(\frac{mg^{1-\frac{1}{n}}L^{\frac{1}{n}}}{g}\right)$	141.55	Freundlich constant (relative adsorption capacity)Freundlich equation exponents
	n	6.68	
	R^2	0.9591	
Temkin	B_T (kJ/mol)	98.2	Temkin constant (heat of sorption)
	K_T (L/g)	12.5	Temkin isotherm constant
	R^2	0.9244	
D-R	q_m (mg g^{-1})	261	Maximum adsorption capacity
	E (kJ mol^{-1})	0.419	Adsorption potential
	R^2	0.6269	

phase) [48]. The isotherm models measure the adsorbent's full capacity, assist in optimizing the adsorption cycle, and provide insight into the mechanisms of the adsorption process. Generally, the act of adsorption is indicated through the mechanism of adsorption isotherm via a description of the adsorption processes. Depending on the isotherm model parameters it might either be monolayer or multilayer adsorption. As shown in Table 3, we discussed the different samples of adsorption isotherm models; Freundlich and Langmuir still are largely used in research work to explain the adsorption act of their adsorbents [49].

Langmuir Adsorption Isotherm Model The equilibrium adsorption isotherm is crucial in the design of an adsorption system because it describes how the solution and the adsorbent interact. It has been discovered that the widely used Langmuir model successfully fits the process. The equation can be written as follows:

$$q_t = \frac{q_m K_L C_e}{1 + K_L C_e} \tag{5}$$

where q_e = the total amount of AR dye adsorbed at equilibrium state (mg/g), c_e denotes the concentration of AR dye solution at equilibrium condition (mg/L), q_m represents the maximum adsorption capacity of AR dye (mg/g), and K_L is the Langmuir isotherm constant. The linear form of the Langmuir equation is:

$$\frac{C_e}{q_e} = \frac{C_e}{q_m} + \frac{1}{q_m K_L} \tag{6}$$

The value of q_e represents a practical limiting adsorption capacity when the surface is fully covered with the dye ions. The values of q_m and K_L are calculated from the slope and intercept of the straight-line plot of $\frac{C_e}{q_e}$ versus C_e (Fig. 9a). In addition, the essential characteristics of Langmuir isotherm can be described by a separation factor (R_L), which is given in the following equation:

$$R_L = \frac{1}{1 + K_L C_e} \tag{7}$$

The value of R_L indicates the shape of the Langmuir isotherm and the nature of the adsorption process. It can give an idea about the nature of adsorption equilibrium: $R_L > 1.0$ unfavorable sorption; $R_L = 1.0$ linear sorption; $R_L < 1.0$ favorable sorption and $R_L = 0$ irreversible sorption. Here, K_L is the Langmuir constant and C_e is the initial concentration of dye. In the study, the value of R_L calculated for the initial concentrations of AR was 0.0018. Since the result is between the ranges of 0–1, the adsorption of AR onto the adsorbent appears to be a favorable process.

Freundlich Adsorption Isotherm Model According to this model, it is used for describing nonideal and reversible adsorption processes, and it may be used to multi-layer adsorption over a heterogeneous surface in which the adsorbent surface is heterogeneous, containing unequal sites for the adsorption of the adsorbate molecules. The model is represented by Eq. (8) [50]:

$$q_e = K_f c_e^{1/n} \tag{8}$$

Equation (8) can be re-written in a linear Eq. (9):

$$\ln q_e = \ln K_f + \frac{1}{n}\left(\ln c_e\right) \tag{9}$$

Here, q_e (mg/g) denotes the amount of dye that got adsorbed on the surface of the adsorbent at equilibrium condition, c_e denotes the concentration of the dye solution at equilibrium condition (mg/L), K_f denotes the adsorption capacity of the adsorbent, and $\frac{1}{n}$ denotes adsorbent intensity. The plot between lnq_e and lnc_e helps to find out K_f and n (Fig. 9b). The type of the isotherm depends on the value of 1/n which
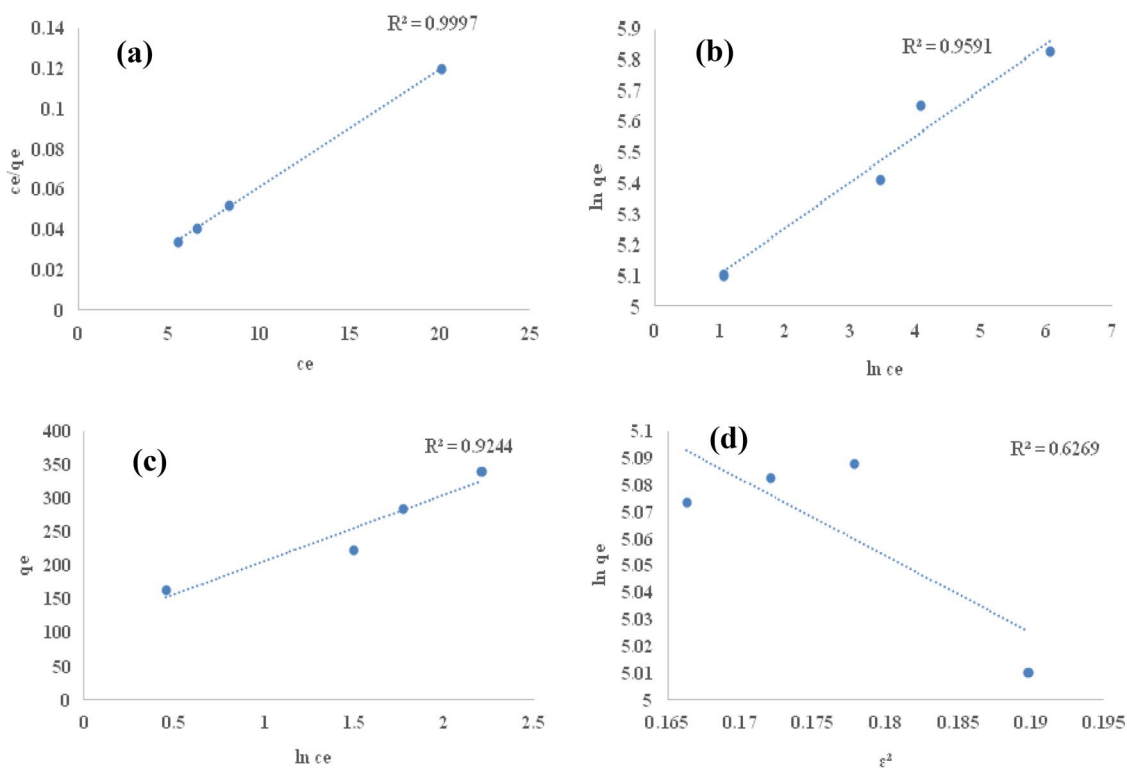
Fig. 9 Asorption isotherm models for AR adsorption by AOC@MC **a** Langmuir isothermmodel **b** Frendlish isotherm model **c** Temkin isotherm model **d** D-R isotherm model

is in the range of 0 and 1. It considers the prediction of the intensity of adsorption or surface heterogeneity, as the value is closer to 0, the surface becomes more heterogeneous, the n value varies with the adsorbent heterogeneity, if n < 10 and n > 1 ,this indicates the favorability. As shown in Table 3, all parameters of the Langmuir and Freundlich isotherms are presented and this demonstrates that the correlation coefficients (R^2) value derived from the longmuir model was higher. As a result, AR adsorption onto the produced material was a monolayer reaction, and the longmuir model was better at predicting the adsorption behavior.

Temkin Adsorption Isotherm Model According to Temkin this model, the adsorption is indicated by the intermolecular attraction between the adsorbate–adsorbent moieties as well as the adsorption heat. The Temkin equation has been represented as: $q_e = B_T \log K_T + B_T \log C_e$ Where, B_T = Temkin constant associated with the adsorption heat (kJ/mol), K_T = Temkin isotherm equilibrium binding constant (L/mg). The graph was obtained from the q_e Vs log C_e plot (Fig. 9c).

Dubinin-Radushkevich (D-R) Adsorption Isotherm Model This model depends on the temperature that indicates if the type of adsorption mechanism is going on

chemically or physically through the energy distribution on a heterogeneous surface (Fig. 9d). It supposes that the adsorbent has no homogeneous surface, and the equation is as follows [51]:

$$\ln q_e = \ln q_m - B\varepsilon^2 \tag{10}$$

$$\varepsilon = RT \ln \left[1 + \frac{1}{C_e} \right] \tag{11}$$

$$E = \frac{1}{\sqrt{2B}} \tag{12}$$

where q_e = the total amount of AR dye adsorbed at equilibrium state (mg/g), c_e denotes the concentration of AR dye solution at equilibrium condition (mg/L), q_m represents the maximum adsorption capacity of AR dye (mg/g), and through Eq. (10) B, is the energy constant of adsorption, that is derived by graphing ln q_e against ε^2. Polanyi potential (ε) is calculated via Eq. (11). R represents the gas constant (8.314×10^{-3} kJ mol^{-1} K^{-1}) and T is the absolute temperature. E (KJ/mol) is the mean free energy of the adsorption is calculated according to Eq. (12). When E < 8 kJ mol^{-1}, physical sorption occurs while E value is 8–16 kJ mol^{-1} a

chemical sorption occurs[52]. Results indicate that AOC@MC shows physical adsorption nature with free energy "E" less than 8 KJ/mol.

(Fig. 9a–c) shows the different types of adsorption isotherm models that were evaluated; the Langmuir Isotherm model, Freundlich isotherm model, Temkin isotherm model and Dubinin-Radushkevich (D-R) model. It has been observed from Table 3 that the adsorption of AR dye on the surface of AOC@MC has been distributed homogenously and show the best fit curve at Langmuir Isotherm model following the pseudo second-order kinetics ($R^2 = 0.999$) as compared to the isotherm analysis study utilizing the model representing the plot by Freundlich Isotherm ($R^2 = 0.9591$), Temkin Isotherm ($R^2 = 0.9562$), and D-R isotherm ($R^2 = 0.6269$).

Effect of AR Initial Concentration and Adsorption Equilibrium Isotherms In a series of flasks containing 0.03 g of AOC@MC composite was added to 25 mL of AR with different concentrations (100, 200, 300 and 400 mg/L). The mixture was then agitated at 250 rpm and 30 $^{\circ}$C for 50 min before being filtered out. The earlier technique was used to determine the dye's residual concentration. The Langmuir and Freundlich were used to evaluate the findings of the influence of AR starting concentration on adsorption capacity in accordance with the formulae presented in (Table 3). The effect of AR concentration on the sorption process before and after the addition of AOC@MC at pH from 1.0 to 7.0 is shown via live pictures in (fig. S8–fig. S11).

Desorption and Reusability Study

Hydrochloric acid 0.5 M was used as an eluent in desorption of Alizarin Red ions from the surface of chitosan composite (Fig. 10). Over three cycles, all composites displayed a moderate adsorption/desorption performance, with ch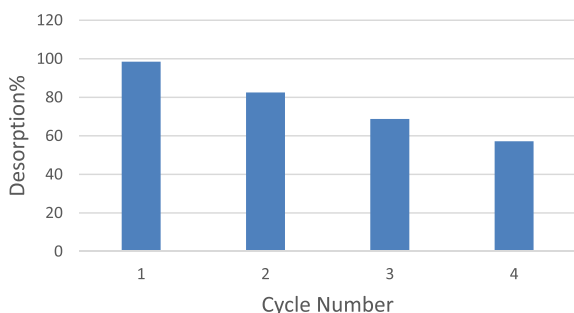anges in adsorption/desorption ability reaching 12%. Desorption ratios were reported as 98.5, 82.5, 68.75, 57.2% respectively.

Antibacterial Activity

The emergence of antibiotic-resistant microbes is a growing concern in the medical community [53]. To combat this issue, researchers are focused on developing new active compounds that can effectively target and eliminate these resistant bacteria [54]. One approach to achieve this via the synthesis of new compounds that possess unique structures and mechanisms of action. This involves designing and testing various chemical structures, which can be modified to enhance their efficacy against resistant bacteria while reducing their toxicity to human cells [55]. The development of active compounds with antibacterial properties can further enhance the effectiveness of dye removal from wastewater [13]. Combining the properties of active compounds used in dye removal and antibacterial activity can lead to the development of innovative and sustainable approaches for wastewater treatment [56]. The use of active compounds with antibacterial properties in dye removal can reduce the use of harmful chemicals and promote environmentally friendly practices.

In the current study, the activity of synthesized sorbent AOC@MC and its heterocyclic base AOC to inhibit the growth of pathogenic bacteria, *S. aureus* and *K. pneumoniae* were investigated using the disk diffusion method. Interestingly, the solvent system (DMSO) did not exhibit any activity against Gram-positive and Gram-negative bacteria. The non-modified and modified sorbent (AOC and AOC@MC, respectively) exhibited promising activity with varied clear zones. The zone of inhibitions formed toward *S. aureus* and *K. pneumoniae* after treatment with AOC and AOC@MC were (17.5 ± 0.4 and 10.8 ± 0.7 mm) and (20.1 ± 0.2 and 17.6 ± 0.4 mm) respectively. As shown in Fig. 11 the activity of AOC@MC is greater than the activity of AOC. This phenomenon could be attributed to the presence of magnetite nanoparticles. In a recent study, the functionalized chitosan with magnetite nanoparticles
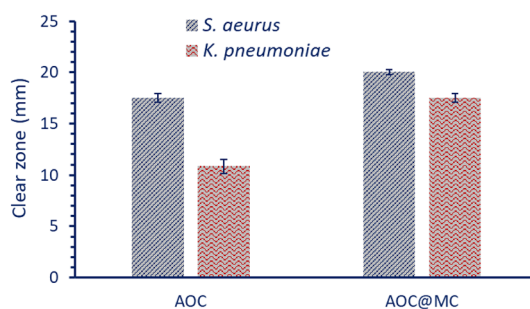

Fig. 10 Reusability study of AOC@MC

Fig. 11 Antibacterial activity of AOC and AOC@MC

showed antimicrobial activity against Gram-positive and Gram-negative bacteria higher than those of non-functionalized ones [31]. Moreover, the antibacterial activity of chitosan modified with magnetite nanoparticles was better than chitosan and magnetite nanoparticles when applied alone [57].

Conclusion

A new modified heterocyclic-magnetite chitosan nanocomposite labeled as AOC@MC was synthesized as a sorbent for removing Alizarin Red dye from aqueous solutions. The prepared sorbent was characterized by FTIR, TGA, TEM, SAED pattern, XRD and SEM-EDX, while the corresponding heterocyclic compounds were characterized by 1 H-NMR and FTIR analysis. The sorption efficiency was tested as a function of time at different pH values and different temperatures. The optimum values were pH = 3.0, contact time = 50 min, and adsorbent dosage = 0.03 g/L at 30 °C. The maximum adsorption capacity was approximately 162 mg/g Within 50 min, the removal percent under these conditions reached 98.9%. Adsorption isotherms were applied to characterize the adsorption process. The modified sorbent was also tested as an antibacterial agent. Results showed that AOC@MC exhibits promising antibacterial activity.

In our future study, we will evaluate AOC@MC and other related modified polymers as dye removal sorbents via a case study targets collecting samples from industrial area (paints and leather tannery) in which we will also complete the antibacterial evaluation of sorbents as a related study.

Declarations

Competing Interests The authors declare no competing interests.

References

1. Qamar SA, Ashiq M, Jahangeer M, Riasat A, Bilal M (2020) Chitosan-based hybrid materials as adsorbents for textile dyes–a review. Case Stud Chem Environ Eng 2:100021

2. Akanda MR, Al-Amin M, Mele MA, Shuva ZM, Hossain MB, Islam T, Hasan MM, Ema UH (2023) Parameters optimization of Fe3O4 NPs synthesis by Tamarindus indica leaf extract possessing both peroxidase as well as excellent dye removal activity. Heliyon. https://doi.org/10.1016/j.heliyon.2023.e16699

3. Dai K, Zhao G, Kou J, Wang Z, Zhang J, Wu J, Yang P, Li M, Tang C, Zhuang W (2021) Magnetic mesoporous sodium citrate modified lignin for improved adsorption of calcium ions and methylene blue from aqueous solution. J Environ Chem Eng 9(2):105180

4. Vishnu D, Dhandapani B, Authilingam S, Sivakumar SV (2022) A comprehensive review of effective adsorbents used for the removal of dyes from wastewater. Curr Anal Chem 18(3):255–268

5. dos Reis GS, Bergna D, Grimm A, Lima EC, Hu T, Naushad M, Lassi U (2023) Preparation of highly porous nitrogen-doped biochar derived from birch tree wastes with superior dye removal performance. Colloids Surf A 669:131493

6. Sharma B, Dangi AK, Shukla P (2018) Contemporary enzyme based technologies for bioremediation: a review. J Environ Manage 210:10–22

7. Dai Y, Yin L, Wang S, Song Y (2020) Shape-selective adsorption mechanism of CS-Z1 microporous molecular sieve for organic pollutants. J Hazard Mater 392:122314

8. Kausar A, Iqbal M, Javed A, Aftab K, Bhatti HN, Nouren S (2018) Dyes adsorption using clay and modified clay: a review. J Mol Liq 256:395–407

9. Mamba FB, Mbuli BS, Ramontja J (2021) Recent advances in biopolymeric membranes towards the removal of emerging organic pollutants from water. Membranes 11(11):798

10. Krishna LS, Yuzir A, Yuvaraja G, Ashokkumar V (2017) Removal of Acid Blue25 from aqueous solutions using Bengal gram fruit shell (BGFS) biomass. Int J Phytoremediat 19(5):431–438

11. Zare EN, Motahari A, Sillanpää M (2018) Nanoadsorbents based on conducting polymer nanocomposites with main focus on polyaniline and its derivatives for removal of heavy metal ions/dyes: a review. Environ Res 162:173–195

12. Botello-González J, Dávila-Guzmán N, Salazar-Rábago J (2021) New generation of eco-friendly adsorbents for future water purification. Handb Nanomater Nanocompos Energy Environ Appl. https://doi.org/10.1007/978-3-030-36268-3_77

13. Zhou Y, Lu J, Zhou Y, Liu Y (2019) Recent advances for dyes removal using novel adsorbents: a review. Environ Pollut 252:352–365

14. Homaeigohar S (2020) The nanosized dye adsorbents for water treatment. Nanomaterials 10(2):295

15. Fu F, Gao Z, Gao L, Li D (2011) Effective adsorption of anionic dye, alizarin red S, from aqueous solutions on activated clay modified by iron oxide. Ind Eng Chem Res 50(16):9712–9717

16. Destaillats H, Colussi A, Joseph JM, Hoffmann MR (2000) Synergistic effects of sonolysis combined with ozonolysis for the oxidation of azobenzene and methyl orange. J Phys Chem A 104(39):8930–8935

17. Deffo G, Temgoua RCT, Mbokou SF, Njanja E, Tonlé IK, Ngameni E (2021) A sensitive voltammetric analysis and detection of alizarin Red S onto a glassy carbon electrode modified by an organosmectite. Sens Int 2:100126

18. Ghorai S, Sarkar AK, Panda AB, Pal S (2013) Effective removal of Congo red dye from aqueous solution using modified xanthan gum/silica hybrid nanocomposite as adsorbent. Bioresour Technol 144:485–491

19. Saeed A, Sharif M, Iqbal M (2010) Application potential of grapefruit peel as dye sorbent: kinetics, equilibrium and mechanism of crystal violet adsorption. J Hazard Mater 179(1–3):564–572

20. Liao G, Li Q, Zhao W, Pang Q, Gao H, Xu Z (2018) In-situ construction of novel silver nanoparticle decorated polymeric spheres as highly active and stable catalysts for reduction of methylene blue dye. Appl Catal A 549:102–111

21. Bui GT, Wang J-H, Lin J-L (2017) Optimization of micropump performance utilizing a single membrane with an active check valve. Micromachines 9(1):1

22. Masheane ML, Nthunya LN, Malinga SP, Nxumalo EN, Mhlanga SD (2017) Chitosan-based nanocomposites for de-nitrification of water. Phys Chem Earth Parts A/B/C 100:212–224

23. Taka AL, Klink MJ, Mbianda XY, Naidoo EB (2021) Chitosan nanocomposites for water treatment by fixed-bed continuous flow column adsorption: a review. Carbohydr Polym 255:117398

24. Taka AL, Doyle BP, Carleschi E, Fonkui TY, Erasmus R, Fosso-Kankeu E, Pillay K, Mbianda XY (2020) Spectroscopic characterization and antimicrobial activity of nanoparticle doped cyclodextrin polyurethane bionanosponge. Mater Sci Eng: C 115:111092

25. Goci MC, Leudjo Taka A, Martin L, Klink MJ (2023) Chitosan-based polymer nanocomposites for environmental remediation of mercury pollution. Polymers 15(3):482

26. Hamza MF, Wei Y, Althumayri K, Fouda A, Hamad NA (2022) Synthesis and characterization of functionalized chitosan nanoparticles with pyrimidine derivative for enhancing ion sorption and application for removal of contaminants. Materials 15(13):4676

27. Hamza MF, Abdellah WM, Zaki DI, Wei Y, Althumayri K, Brostow W, Hamad NA (2023) A phosphonic functionalized biopolymer for the sorption of lanthanum (III) and application in the recovery of rare earth elements. Sustainability 15(3):2843

28. Kuo P-Y, Sain M, Yan N (2014) Synthesis and characterization of an extractive-based bio-epoxy resin from beetle infested Pinus contorta bark. Green Chem 16(7):3483–3493

29. Hamza MF, Hamad DM, Hamad NA, Adel A-H, Fouda A, Wei Y, Guibal E, El-Etrawy A-AS (2022) Functionalization of magnetic chitosan microparticles for high-performance removal of chromate from aqueous solutions and tannery effluent. Chem Eng J 428:131775

30. Hamza MF, Wei Y, Khalafalla MS, Abed NS, Fouda A, Elwakeel KZ, Guibal E, Hamad NA (2022) U (VI) and th (IV) recovery using silica beads functionalized with urea-or thiourea-based polymers–application to ore leachate. Sci Total Environ 821:153184

31. Hamza MF, Fouda A, Elwakeel KZ, Wei Y, Guibal E, Hamad NA (2021) Phosphorylation of guar gum/magnetite/chitosan nanocomposites for uranium sorption and antibacterial applications. Molecules 26(7):1920

32. Fouda A, Hassan SE-D, Saied E, Hamza MF (2021) Photocatalytic degradation of real textile and tannery effluent using biosynthesized magnesium oxide nanoparticles (MgO-NPs), heavy metal adsorption, phytotoxicity, and antimicrobial activity. J Environ Chem Eng 9(4):105346

33. Vedula SS, Yadav GD (2023) Treatment of wastewater containing alizarin red dye: development and application of magnetic chitosan as a natural eco-friendly material. Clean Technol Environ Policy 25(3):865–878

34. Bajpai O, Panja S, Chattopadhyay S, Setua D (2015) Process–structure–property relationships in nanocomposites based on piezoelectric-polymer matrix and magnetic nanoparticles, manufacturing of nanocomposites with engineering plastics. Elsevier, Amsterdam, pp 255–278

35. Coates J (2006) Interpretation of infrared spectra, a practical approach. Encycl Anal Chem 12(10):815–810

36. Coates J (2000) Interpretation of infrared spectra, a practical approach

37. Pylypchuk IV, Kołodyńska D, Kozioł M, Gorbyk P (2016) Gd-DTPA adsorption on chitosan/magnetite nanocomposites. Nanoscale Res Lett 11(1):1–10

38. Iordache M, Dodi G, Hritcu D, Draganescu D, Chiscan O, Popa M (2018) Magnetic chitosan grafted (alkyl acrylate) composite particles: synthesis, characterization and evaluation as adsorbents. Arab J Chem 11(7):1032–1043

39. Qu W, He D, Guo Y, Tang Y, Song R-J (2019) Characterization of modified Alternanthera philoxeroides by diethylenetriamine and its application in the adsorption of copper (II) ions in aqueous solution. Environ Sci Pollut Res 26:21189–21200

40. Yu C, Geng J, Zhuang Y, Zhao J, Chu L, Luo X, Zhao Y, Guo Y (2016) Preparation of the chitosan grafted poly (quaternary ammonium)/Fe3O4 nanoparticles and its adsorption performance for food yellow 3. Carbohydr Polym 152:327–336

41. Lin-Vien D, Colthup NB, Fateley WG, Grasselli JG (1991) The handbook of infrared and Raman characteristic frequencies of organic molecules. Elsevier, Amsterdam

42. Bloxham S, Eicher-Lorka O, Jakubėnas R, Niaura G (2003) Adsorption of cysteamine at copper electrodes as studied by Surface-Enhanced Raman Spectroscopy. Spectrosc Lett 36(3):211–226

43. Song J, Zou W, Bian Y, Su F, Han R (2011) Adsorption characteristics of methylene blue by peanut husk in batch and column modes. Desalination 265(1–3):119–125

44. Tran Thuy TM, Nguyen DV (2023) Octahedral molecular sieve manganese oxide: feasible material for hg (ii) remediation. Adv Sci Technol 122:35–40

45. Zhuang S, Zhu K, Hu J, Wang J (2022) Selective and effective adsorption of cesium ions by metal hexacyanoferrates (MHCF, M = Cu, Co, Ni) modified chitosan fibrous biosorbent. Sci Total Environ 835:155575

46. Obiora-Okafo IA, Onukwuli OD, Igwegbe CA, Onu CE, Omotioma M (2022) Enhanced performance of natural polymer coagulants for dye removal from wastewater: coagulation kinetics, and mathematical modelling approach. Environ Process 9(2):20

47. Bagtash M, Zolgharnein J (2023) Response surface optimization for simultaneous removal of alizarin red S and alizarin yellow dyes from aqueous solution using magnetic Zn-Al-Zr layered double hydroxide. Inorg Nano-Metal Chem. https://doi.org/10.1080/24701556.2023.2188459

48. Boparai HK, Joseph M, O'Carroll DM (2011) Kinetics and thermodynamics of cadmium ion removal by adsorption onto nano zerovalent iron particles. J Hazard Mater 186(1):458–465

49. Srinivasan A, Viraraghavan T (2010) Decolorization of dye wastewaters by biosorbents: a review. J Environ Manage 91(10):1915–1929

50. Hasan MM, Kubra KT, Hasan MN, Awual ME, Salman MS, Sheikh MC, Rehan AI, Rasee AI, Waliullah R, Islam MS (2023) Sustainable ligand-modified based composite material for the selective and effective cadmium (II) capturing from wastewater. J Mol Liq 371:121125

51. Rudram C, Praveen LP, Reddy PDS (2023) An experimental study on fluoride removal from aqueous solution by using thermally treated annona squamosa with and without presence of the inert gas as adsorbent. Novel Aspect Chem Biochem 2:126–146

52. Inyinbor AA, Bankole DT, Adekola FA, Bello OS, Oreofe T, Amone K, Lukman AF (2023) Chemometrics validation of adsorption process economy: case study of acetaminophen removal onto quail eggshell adsorbents. Sci Afr 19:e01471

53. Ventola CL (2015) The antibiotic resistance crisis: part 1: causes and threats. P&T 40(4):277–283

54. Mohamed AE, Elgammal WE, Eid AM, Dawaba AM, Ibrahim AG, Fouda A, Hassan SM (2022) Synthesis and characterization of new functionalized chitosan and its antimicrobial and in-vitro release behavior from topical gel. Int J Biol Macromol 207:242–253

55. Wright GD (2016) Antibiotic adjuvants: rescuing antibiotics from resistance. Trends Microbiol 24(11):862–871

56. Dan S, Bagheri H, Shahidizadeh A, Hashemipour H (2023) Performance of graphene Oxide/SiO2 Nanocomposite-based: antibacterial activity, dye and heavy metal removal. Arab J Chem 16(2):104450

57. Haldorai Y, Kharismadewi D, Tuma D, Shim J-J (2015) Properties of chitosan/magnetite nanoparticles composites for efficient dye adsorption and antibacterial agent. Korean J Chem Eng 32(8):1688–1693